Accepted Manuscript

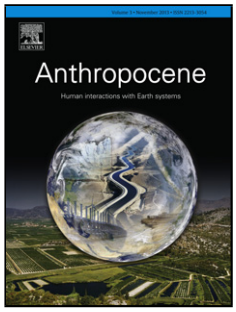

Title: Anthropogenic overprints on natural coastal aeolian sediments: a study from the periphery of ancient Caesarea, Israel

Authors: Gilad Shtienberg, Justin K. Dix, Ruth Shahack-Gross, Assaf Yasur-Landau, Joel Roskin, Revital Bookman, Nicolas Waldmann, Sariel Shalev, Dorit Sivan

PII: S2213-3054(17)30013-9
DOI: http://dx.doi.org/10.1016/j.ancene.2017.08.004
Reference: ANCENE 148

To appear in:

Received date: 12-2-2017
Revised date: 13-8-2017
Accepted date: 17-8-2017

Please cite this article as: Shtienberg, Gilad, Dix, Justin K., Shahack-Gross, Ruth, Yasur-Landau, Assaf, Roskin, Joel, Bookman, Revital, Waldmann, Nicolas, Shalev, Sariel, Sivan, Dorit, Anthropogenic overprints on natural coastal aeolian sediments: a study from the periphery of ancient Caesarea, Israel.Anthropocene http://dx.doi.org/10.1016/j.ancene.2017.08.004

Anthropogenic overprints on natural coastal aeolian sediments: a study from the periphery of ancient Caesarea, Israel

Gilad Shtienberg[a,*], Justin K. Dix[b], Ruth Shahack-Gross[a,c], Assaf Yasur-Landau[a,c], Joel Roskin[c,d,e], Revital Bookman[e], Nicolas Waldmann[e], Sariel Shalev[a,f], Dorit Sivan[a,c]

[a] *Department of Maritime Civilizations, L.H. Charney School of Marine Sciences, University of Haifa, Haifa 3498838, Israel*

[b] *The School of Ocean and Earth, University of Southampton, Southampton SO14 3ZH, UK*

[c] *The Recanati Institute for Maritime Studies (RIMS), University of Haifa, Haifa 3498838, Israel*

[d] *The School of Sciences, Achva Academic College, Israel*

[e] *Dr. Moses Strauss Department of Marine Geosciences, L.H. Charney School of Marine Sciences University of Haifa, Haifa 3498838, Israel*

[f] *Department of Archaeology, University of Haifa, Haifa 3498838, Israel*

Abstract

Near surface sediment stratigraphy associated with ancient human settlements can potentially reveal the complex history of human impact. This study explores such impacts in the area around ancient Caesarea, a well-known Roman to Early Islam period metropolis in the central coastal plain of Israel, with analysis of human-induced macro-features and microscopic remains found in buried sediments. We retrieved these anthropogenic markers through boreholes and analysed them with sedimentological and radiometric dating techniques, integrated with archaeological and historical records. The analysis identified a refuse deposit comprising two grey loamy sand artefact-bearing facies bedded between late Holocene aeolian sand. One anthropogenic facies represents an urban garbage mound and the other may be an agricultural pedo-sediment, both dated to the Roman to Early Islamic periods. The grey pedo-sediment, contained in three boreholes in the lowlands south of Caesarea, covers an area of at least 1.4 km^2. Apparently improved in terms of soil fertility, we postulate that the pedo-sediment is the outcome of composting enrichment of the soil for agriculture. Taking advantage of the high coastal freshwater aquifer in the study area, we propose that the pedo-sediment represents buried agricultural plots. The comprehensive, multi-disciplinary approach demonstrated in this study of cored sediments outside ancient human settlements is among the few in the coastal area of the southern Levant. It could be relevant to other archaeological sites in the Mediterranean and elsewhere around the world.

Keywords

Eastern Mediterranean; pedo-sediment, anthropogenic traces; Islamic period, Caesarea hinterlands, aeolian coastal sand.

1. Introduction

For millennia, humans have manipulated soils for habitation purposes, leading to changes in the physical and chemical properties (Bouma and Hole, 1971; Hole, 1974; Nicosia and Devos, 2014). Therefore, a complex history of human impact on the environment is accruing in sediments and soils. Extensive archaeological and paleoenvironmental research has increased the understanding that significant human perturbations to the landscape occurred throughout hominin evolution, most significantly with the advent of agriculture (Sandor et al., 1990; Certini and Scalenghe, 2011; Zeder, 2011).

In the southeast Mediterranean coastal region, the Holocene period is characterized by ongoing interaction between natural processes and human activities (Bar-Yosef, 1975; Galili and Nir, 1993; Galili et al., 1993; Godfrey-Smith et al., 2003). Anthropogenic activities that have impacted the environment include site construction, animal domestication, wood/charcoal burning and cultivation of crops. Human activity has left distinct traces in soils such as macroscopic artefacts: pottery, stone tools, architecture and bone remains. Microscopic evidence of human activity includes livestock dung spherulites, ash and micro-charcoal, phytoliths (plant-made minerals which may be preserved in soils and sediments) and enrichment of certain elements (i.e., phosphorous and sulphur) (Weiner, 2010). Techniques used to identify anthropogenic impacts in soils are usually applied to settlement sites and rarely to cultivated hinterlands (Smejda et al., 2017).

This study focuses on the area to the south of ancient Caesarea, Israel (32°30’0” N, 34°53’30” E), a well-known Roman to Crusader period (31 BCE to 1265 CE) urban centre. The continuous efforts of the local population to adapt their activities to both their varying needs

and changing natural environments has resulted in human-induced landscape changes, giving rise to a complex cause-effect phenomena (Ackermann et al., 2014, 2015). This study investigates the effect of human settlement on the proximate environment, outside the settlement itself, through analysis of anthropogenic markers present within the local sediment stratigraphy. We identified markers through a combination of sedimentological, petrophysical, geochemical, chronological and microarchaeological analyses conducted on four boreholes. Integration of these new data with extant topographical data, borehole records, established chronology, archaeological finds and historical documentation, resulted in a spatially extensive interpretation of changing settlement and subsistence patterns in the area.

2. The study area

The study area is located in the Caesarea lowlands (Shtienberg et al., 2017), situated in the centre of the 190 km-long coastal plain of Israel (Fig. 1a, b). The study area extends up to 1.5 km east from the Mediterranean Sea between Hadera Stream to the south and Caesarea to the north. South of Haifa Bay, the coastal plain of Israel is dominated by Nile-derived quartz sand deposits attaining thicknesses of 1 to 9 m (Neev et al., 1978; Almagor et al., 2000; Zviely et al., 2006; Schattner et al., 2010; Roskin et al., 2015, 2017; Shtienberg et al., 2016). Longshore currents transported this allogenic material to the region throughout the Quaternary period (Fig. 1a; Picard, 1943; Emery and Neev, 1960; Pomerancblum, 1966; Zviely et al., 2009; Davis et al., 2012). Wave- and wind-induced currents transported the sediments to the beach, and wind carried them inland to form sand sheets and dunes (Fig. 1b). The quartz sand eventually formed the Late Pleistocene sequence consisting of alternating aeolianites (cemented dune sand locally known as `*kurkar*') and red-brown silty clayey sandy loams (Palaeosols) overlain by loose sand

sheets and dunes (Fig. 1b; Yaalon, 1967; Yaalon and Dan, 1967; Gvirtzman et al., 1998; Frechen et al., 2002; Sivan and Porat, 2004; Mauz et al., 2013). Aeolianites in the vicinity of Caesarea are chronologically constrained between approximately 115 and 50 thousand years ago (ka; Engelmann et al., 2001; Frechen et al., 2004; Sivan and Porat, 2004; Sivan et al., 2004; Mauz et al., 2013; Shtienberg et al., 2017). The overlying palaeosol units, reaching a maximum thickness of 8 m, date from roughly 100 to 8 ka (Gvirtzman and Wieder, 2001; Frechen et al., 2001; Roskin et al., 2015; Shtienberg et al., 2017), indicating they are sometimes synchronous with aeolianite formation (Sivan and Porat, 2004) and sometimes younger. As sea level rose during the Late Pleistocene-Holocene transition, the shoreline migrated eastwards, flooding the shallow shelf (depth shallower than -20 m) c. 8 ka (Sivan et al., 2001, 2004). The Nilotic sands accumulated on the coast, initially covering the palaeosol surface c. 7 ka (Frechen et al., 2002; Porat et al., 2004; Mauz et al., 2013; Shtienberg et al., 2017). By 1.2 to 1.1 ka, the sand reached its easternmost extent in the Caesarea hinterland and stabilized shortly afterwards (Roskin et al., 2015).

The study area experiences a sub-humid Mediterranean climate characterized by a hot, dry summer season (June to September) and a cool, rainy winter season (December to February). The mean temperature in January and August is 12 ºC and 26 ºC, respectively. The rainy season generally lasts from October to May, with a mean annual rainfall of 500–600 mm (Israel Meteorological Service, 2011). This climate regime has generally prevailed during the last 3,000 years with only modest fluctuations (Bar-Matthews et al., 2003; Revel et al., 2010; Langgut et al., 2011; Ellenblum, 2012) and thus is relevant to the historical periods discussed in this study. Vegetation cover mainly consists of Mediterranean garrigue and maquis

vegetation (Danin, 2005) that likely contributed to the stabilization of sands and dunes (Levin, 2013; Roskin et al., 2015).

In the vicinity of Caesarea (Fig. 1c), the earliest historical settlement is attributed to the Persian period at approximately 400 BCE (Raban, 2007). Known as "Straton's Tower" (Stieglitz, 1996), the settlement was completely rebuilt during the reign of Herod the Great and renamed Caesarea in honour of the Roman Emperor Augustus Caesar (Patrich, 2001; Porath, 2002; Reinhardt and Raban, 2008; Table 4 in Roskin et al., 2015). Throughout the Roman and Byzantine periods (31 BCE to 640 CE), the city functioned as a provincial metropolis (Reinhardt and Raban, 1999, 2008; Goodman-Tchernov and Austin, 2015). Caesarea reached its maximum extent (1.2 km^2) by the 5^{th} and 6^{th} centuries CE, housing a population of 25,000 to 35,000 (Holum, 2011). During the late Roman to Byzantine period, a lively export and import trade passed through Caesarea's harbor. Local markets included agricultural products such as wheat, dates, rice and cumin cultivated in the city's territory (Habas, 1996; Holum, 2009). Caesarea was conquered by the Muslim Rashidun army under 'Amr ibn al-'As's leadership during the 7^{th} century CE; however, the population did not decrease significantly. Furthermore, archaeobotanical and historical evidence suggest that Islamic Caesarea significantly invested in local agriculture (Holum, 2011). During the 11^{th} Century CE, Caesarea was taken by the Crusaders, resulting in decline of the city, reduction of population, and a change of settlement pattern from urban to rural (Taxel, 2013; Avni, 2014; Ramsay and Holum, 2015).

Although few known archaeological sites (i.e. farming complexes and irrigation systems) surround Caesarea (Fig. 2; Olami et al., 2005; Ad, 2009), Roman, Byzantine and Islamic period glass and pottery remains are scattered on the sand surface (Fig. 2e). These remains cover rectangular to square areas defined by low sand berms (Fig 2c, d) that may be associated with

Mawasi agriculture (Porath, 1975), a traditional-farming practise that takes advantage of the coastline's high fresh water table (Tsoar and Zohar, 1985).

Based on historical documentation of Caesarea's urban development and findings in nearby cities, we hypothesized that areas to the south of Caesarea were cultivated to support the urban population during its prime, from the Roman-Byzantine period until Early Islamic times. This study tests the hypothesis by investigating the following questions:

1. Is there an environmental signature within the sediments of Caesarea's hinterland that is compatible with extensive agricultural activity?
2. Was active cultivation present throughout the Roman period to the Crusader period?
3. Assuming the city was supported by an agricultural hinterland, how did cultivation take place in the nutrient-deprived, sandy sediments characterized by poor water adhesion properties?

3. Materials and Methods

In order to answer the research questions, we combined detailed analyses of four new boreholes with a large extant database of cores taken across the area for both academic and industrial purposes.

3.1 Compilation of existing data sets

We compiled published logs from 70 existing boreholes (Fig. 1c; supplements) and converted the borehole locations, elevations, and lithological descriptions to a common coordinate system (WGS84-UTM 36N) and vertical datum (Israel Land Survey Datum; ILSD) system in ArcGIS. The ArcGIS database also contained existing digital elevation models (DEMS; 4 × 4 m bin size), soil maps, rectified aerial photographs and chronostratigraphic data. We generated topographic and isopach surface for each facies and mapped to a bin size of 25 ×

25 m through interpolation, using the ArcGIS *Topo to Raster* module (Fig. 3). This procedure uses an iterative finite difference interpolation technique that allows the fitted DEM to follow abrupt changes in terrain, such as streams, ridges and cliffs.

3.2 New borehole drilling and petro-sedimentological analyses

We chose the locations of the new boreholes based on interpretation of the ground model developed from extant logs, focusing on horizons with high potential of anthropogenic activity as indicated by anecdotal records of artefacts. (Fig. 3c). Coring was completed with a Geo-probe 6620DT direct push corer in the high potential zones up to 1.5 km inland of the Mediterranean Sea. We measured the locations and elevations of the four boreholes using a Proflex 500 RTK-GPS with precision of ± 1 cm and ± 5 cm, respectively (Fig. 1c). The cores were then sectioned lengthwise to describe colour (Munsell colour chart) and lithology. Digital photographic analysis of the sediments assigned brightness values ranging from 0 to 254 for each pixel.

We measured magnetic susceptibility (MS) and density of the cores at every 2 cm. The measurements were made by a Geotek multi-sensor core logger equipped with a Bartington loop sensor compatible with small diameter cores. Using a Beckman Coulter LS 13 320 Laser diffraction Particle Size Analyzer, we carried out particle size distribution (PSD) analysis on 95 samples prepared by consolidating representative sediments of the four main lithofacies that were identified. Petrographic observations were made using an Olympus BX53-P petrographic microscope, following Wright and Tucker (1991),Wright (1992) and Adams and Mackemzie (1998). Total organic carbon (TOC) and inorganic carbon (IC) of 75 freeze-dried sediment samples were measured with a PrimacsSLC TOC Analyzer. X-ray fluorescence (XRF) analysis was completed on 90 samples using the EX-310LC(ED) instrument in an excitation voltage of

35 kV with beam diameter of 8 mm. The raw element values were then normalized to silica values, a dominant element in Israel's coastal sediments, to enable relative difference assessment for each sub-unit sample (Revel et al., 2010; Box et al., 2011).

We determined the mineralogical composition of the identified litho-facies through Fourier Transform Infrared spectroscopy (FTIR) analysis using a Nicolet iS5 FTIR spectrometer and ''Omnic'' software. After homogenization by grinding, bulk sediment samples were prepared using the KBr method. Interpretation of the mineralogical composition was based on reference libraries.

3.2 Dating

3.2.1 Optically Stimulated Luminescence

One optically stimulated luminescence (OSL) sample was prepared and measured at the Luminescence Laboratory of the Geological Survey of Israel, Jerusalem. Quartz grains (125–150 μm) were extracted using routine laboratory procedures under subdued orange light (Davidovich et al., 2012), following single aliquot regenerative-dose (SAR) protocol. Further data on OSL procedures performed on aeolian sand by the Geological Survey of Israel can be found in Shtienberg et al., 2017. OSL ages are presented in thousands of years (ka) before 2015 (Table 2).

3.2.2 Radiocarbon

Four samples (one bone and three wood fragments) were ^{14}C-dated using the Accelerator Mass Spectrometry (AMS) technique (Table 2; Fig. 1c). The samples were selected following pre-screening using FTIR spectroscopy. Samples were pre-treated, graphitized and measured at the Poznan radiocarbon laboratory in Poznan, Poland. The ages obtained are given as ^{14}C age ±

1σ year before present (BP), and the calibrated ranges for ± 1σ and ± 2σ in years BP, according to the convention in Stuiver and Polach (1977). Radiocarbon dates were calibrated using the IntCal 13 atmospheric curve (Reimer et al., 2009) and OxCal version 4.2.3© (Ramsey and Lee, 2013).

4. Results

The stratigraphy of the area to the south of Caesarea consists of two main units: F1 and F2 (Table 3; Figs. 4, 6), which can be divided into one and four facies, respectively. The lithological characteristics of each unit and correlations between the boreholes were described through integration of their sedimentological properties with mineralogy, petrographic microscopy and elemental composition.

4.1 Unit F1

Unit F1 is found in all four cores. It is composed of approximately 65 % sand, 25 % silt, and 10 % clay. F1 consists of very low values (<0.1 %) of $CaCO_3$ and TOC. Brightness values vary from 70 to 150, while colour is dark reddish brown to dull brown (2.5YR3/3 to 7.5YR4/5). MS values range from 60 to 150 $\times 10^{-8}$ m^3 Kg^{-1} (Fig. 4). Microscopically, F1 comprises well-sorted, sub-rounded to rounded quartz grains within a groundmass of reddish brown clay, and is barren of phytoliths (Fig. 5a). Mineralogically, it is composed of quartz and clay. The unit is relatively enriched in the elements P, Fe, Al, Ti, Zn and Sr (analysed in core SDC2) compared to the unit immediately above it, facies F2a (Fig. 6). Based on the relatively high MS values, hue, granulometry ratios and microscopic features this unit is interpreted as a palaeosol.

4.2 Unit F2

Unit F2 lies unconformably over unit F1 and consists of four facies: F2a, F2b (1-3), F2c and F2d (Fig. 4).

4.2.1 Facies F2a

Facies F2a is found in all four cores (Fig. 4). It is composed of roughly 85 % sand, 10% silt, and5 % clay. $CaCO_3$ concentrations range between 0 to 20 %, and TOC values are higher than unit F1 (< 0.8 %). Brightness values vary from 150 to 220, and colour is pale yellow to light grey (2.5Y 8/1 to 5Y8/2). MS values range from 25 to 50 $\times 10^{-8}$ m^3 Kg^{-1}. F2a consists of well-sorted, sub-rounded quartz grains and bioclasts, including bivalve shells, land snail fragments and foraminifera species of the family Textulariidae. No phytoliths were evident (Fig. 5b). Elemental concentrations in F2a (analysed in cores SY1, SDC1 and SDC2) are the lowest compared to F1 and facies of F2b and F2c (Fig. 6). The mineral composition of F2a includes quartz, aragonite and calcite from sand, shell and microfossil remains, respectively (Fig. 4). Based on the facies, granulometry ratios, hues and microscopic features this facies is interpreted as aeolian sand.

4.2.2 Facies F2b

Facies F2b is identified in borehole SY1 south of ancient Caesarea, and includes three sub-facies (F2b1; F2b2; F2b3) that are separated by facies F2a (Fig. 4). These facies are all greyish in colour:

1. Sub-facies F2b1 is 1.2 m thick and consists of about 80 % sand, 15 % silt and 5 % clay. $CaCO_3$ concentrations range from 0 % to 20 %, while TOC values are as high as 0.4 %. F2b1 has a brightness value of 150, and colour is light greyish yellow (2.5Y 7/3). MS values mostly range from 50 to 80 $\times 10^{-8}$ m^3 Kg^{-1}. Phytoliths, pottery remains, 1 cm calcareous sandstone

clasts, wood pieces, shell and glass fragments (> 1 cm) are present throughout this poorly-sorted sub-facies (Fig. 5b, c, f1-2). F2b1 mainly consists of quartz, calcite and aragonite with the carbonated phosphate mineral hydroxylapatite identified 0.15 m above its base (Fig. 4). Hydroxylapaite is a major component of bone, but may also form diagenetically following composting processes (Weiner, 2010). Elemental analysis shows high concentrations of P, Fe, Ca, Ti and Pb compared to F2a, peaking about 0.4 m from the sub-facies surface (Fig. 6). Two wood fragments sampled 0.1 and 0.35 m below the sub-facies surface were radiocarbon dated to 1960 with a probability of 95 % (Table 2). These two samples and a third wood fragment collected in facies F2c likely represent modern vegetation roots that penetrated deep into the subsurface (Kutiel et al., 2016). Based on the elemental and mineral composition, hues and microscopic and macroscopic features this sub-facies is interpreted to be an anthroposol.

2. Sub-facies, F2b2 is 1 m thick and is composed of 80 % sand, 15 % silt, and 5 % clay. $CaCO_3$ concentrations range from 12 % to 25 %, and TOC values fluctuate from 0.2 % to 0.8 %. Brightness values are around110, and colour is light grey (10Y 7/1). MS values mostly range from 50 to 180 $\times 10^{-8}$ m^3 Kg^{-1}, peaking 0.6 m below the sub-facies surface (Fig. 4). The sub-facies is poorly-sorted with pottery remains, 1 cm calcareous sandstone clasts and shells present throughout. Bone fragments were identified 0.2 to 0.3 m below the F2b2 surface (Fig. 5b). F2b2 consists of quartz, calcite and carbonated hydroxylapatite minerals. Microscopically, it was found to contain micritic calcite that resembles wood ash (Shahack-Gross and Ayalon, 2013), phytoliths and micro-charcoal fragments. Quartz grains appear to be less frequent than in the overlying upper section (Fig. 5b, c). Concentrations of P, Fe, Al, Ca, Ti, Zn, Cu, and Pb are highest in F2b2 compared to all other sub-facies and facies across

the boreholes. Elemental concentrations peak 0.6 m below the sub-facies surface (Fig. 6). A 1.5 × 1.5 cm bone fragment found in F2b2 was dated between 1354 and 1242 calibrated years BP (Table 2; Fig. 6), i.e., the Early Islamic period. Based on the elemental and mineral composition, hues and microscopic and macroscopic features this sub-facies is interpreted as an anthroposol.

3. Sub-facies F2b3 is 1.5 m thick. It is composed of approximately 90 % sand, and 0 % silt. The $CaCO_3$ concentration of is about 8 %, while TOC values range from 0.3 % to 0.6 %. Brightness values are 150, and colour varies from light grey to yellowish grey (10Y 7/2 to 2.5Y 5/1). MS values mostly range from 80 to 250 $\times 10^{-8}$ m^3 Kg^{-1} (Fig. 4). We identified small pottery remains (> 2 cm; Fig. 5f), 1 cm calcareous sandstone clasts, land snail and bivalve shell fragments throughout this poorly-sorted sub-facies. Minerals identified in F2b3 include quartz, calcite, aragonite and carbonated hydroxylapatite. Microscopically, the sub-facies consists of micritic calcite (ash), phytoliths and micro-charcoal fragments (Fig. 5b, c). Concentrations of P, S, Fe, Al, Ti and Pb are comparatively high. A peak was identified for Ca, Zn and Cu at 0.3 m below F2b3's surface (Fig. 6). Based on elemental and mineral composition, hues and microscopic and macroscopic features this sub-facies is interpreted to be an anthroposol.

4.2.3 Facies F2c

Facies F2c is identified in boreholes SDC1, SDC2, SDC4, covering unit F2a with thicknesses of 1 to 2 m. It is composed of roughly 85 % sand, and 15 % silt. $CaCO_3$ concentrations are between 5 % and 12 %, while TOC values fluctuate from 0 % to 0.4 %. Brightness values vary from 130 to 200, and colour is yellowish grey to light grey (2.5Y 5/1 to 10YR 8/1). MS values mostly range from 30 to 80 $\times 10^{-8}$ m^3 Kg^{-1} (Fig. 4). Microscopic

examination identified traces of phytoliths and subrounded quartz grains surrounded by dark microsparitic calcite (Fig. 5d). We identified pottery fragments, 0.5 cm calcareous sandstone clasts, shell and land snail fragments, wood remains and small glass fragments (> 1 cm) throughout the facies. F2c is relatively well sorted and consists of quartz, aragonite, calcite and carbonated hydroxylapatite minerals. Elemental concentrations of P, S, Fe, Al, Ca, Ti, Zn, Sr and Pb are higher compared to F2a but lower compared to F2b. One OSL age (sample HAD-90; Table 1) dated F2c to 0.85 ± 0.11 ka (1165 ± 110 CE – the Crusader period). The sample was collected 200 m east of the Mediterranean Sea, 0.7 m below the facies surface (Fig. 7). A wood fragment sampled 0.15 m below the F2c surface in borehole SDC1 was dated to 1960 with a probability of 95 % (Table 2). Based on the elemental and mineral composition, hues and microscopic and macroscopic features this facies is interpreted to be an anthroposol.

4.2.4 Facies F2d

F2d is the topmost facies in boreholes SDC1, SDC2 and SDC4 (Fig. 4). It is composed of about 95 % sand and ~5 % silt. $CaCO_3$ concentrations range from 6 % to 15 %, while TOC values fluctuate between 0 % and 0.6 %. Brightness values vary from 180 to 200, and colour is light grey to pale yellow (5Y 8/1 to 5Y8/4). MS values mostly range from 15 to 25 $\times 10^{-8}$ m^3 Kg^{-1}. F2d consists of well-sorted, sub-rounded quartz grains sometimes accompanied by land snail shell fragments. F2d is free of sherds, calcareous sandstone clasts, glass fragments and barren of phytoliths wood ash and micro-charcoal. Elemental concentrations in cores SDC1 and SDC2 resemble those of F2a and are comparatively lower than concentrations measured in unit F1 and facies F2b and F2c (Fig. 6). Mineralogically, F2d is composed of quartz, aragonite and calcite from sand and shell remains greater than 0.5 cm (Fig. 4). Based on the granulometry ratios, hues and microscopic features this facies is interpreted as aeolian sand.

5. Discussion

We combined detailed analyses of four newly acquired boreholes with a chronologically constrained ground model generated from extant datasets to answer questions regarding the nature of human-landscape activity in the hinterland to the south of Caesarea.

5.1 Palaeo-topography spatial variability and chrono-stratigraphy

The base lithology underlying the study area consists of aeolianites and palaeosols that range between elevations of -4 to +7.8 relative to the Israel Land Survey Datum (mILSD; Fig. 3a). We identified four sand facies (Figs. 1c, 6; Table 3) overlying the basal topography (Fig. 7; Table 3). Sand accumulations up to 9 m thick (Fig. 3a) fill the base topographic lows while the thinnest accumulations, about 0.5 m thickness, overlay topographic highs.

OSL (Roskin et al., 2015) and infrared stimulated luminescence (IRSL; Frechen et al., 2002) techniques dated the lower aeolian sand facies (F2a) to 5.9 – 3.3 ka (Fig. 7). F2a covers most of the basal topography between Hadera and Caesarea (Fig. 1c). Based on these ages and previous studies conducted on the north central coast of Israel (Kadosh et al., 2004; Porat et al., 2004; Cohen-Seffer et al., 2005; Mauz et al., 2013; Shtienberg et al., 2017), the initial aeolian sand incursion and stabilisation of the coastal landscape occurred around 3885 ± 900 BCE (Fig. 7), i.e. the Chalcolithic period.

Overlying F2a is a grey coloured, artefact-containing pedo-sediment (facies F2b and F2c; Table 3) that was mapped (Figs. 1c, 3c) throughout the southern parts of Caesarea's lowlands (Shtienberg et al., 2017). This grey sand is identified in the vicinity of high sand berms (Fig. 2), covering an area of 1.4 km^2 that extends up to 3 km south of the city boundaries. These facies thin with distance from Caesarea. The results of this study indicate these facies are

chronologically constrained between 662 CE and 1165 ± 110 CE, i.e., Early Islamic to Crusader period (Table 3). These results are supported by a previously published OSL date of 1165 ± 110 CE from the dune field located 3 km south of the city (Fig. 7; Roskin et al., 2015).

The anthropogenic sand facies F2b and F2c are covered by yellow aeolian sand (F2d) that was deposited after 1165 ± 110 CE, i.e., the Crusader period. During the Crusader period, the city of Caesarea was under constant attack, resulting in declining human presence in the area south of Caesarea (Porath, 2000). The decrease in human activity caused re-establishment of vegetation and sand stabilization. Based on ages from the same facies on the adjacent coastal plain and coastal escarpment (Fig. 1c; Frechen et al., 2001; Salmon, 2013; Roskin et al., 2015), we propose that the upper sand (F2d) was deposited and stabilized from 1365 ± 160 CE until present. This combined chronology is consistent with the archaeological and historical timelines of ancient Caesarea (Table 3).

5.2 Anthropogenic activity in the outskirts of ancient Caesarea

The grey facies F2b and F2c have a typical anthropogenic pedo-sediment composition previously identified in prehistoric (Shahack-Gross et al., 2004) and historic (Regev et al., 2015) sites. The composition of F2b and F2c reflects the past presence of organic matter and/or bones; ash, micro-charcoal and high MS values corresponding with fire; plant phytoliths; and macroscopic artefacts such a pottery and glass. Due to their size (< 2 cm), the macroscopic artefacts do not enable further investigation. All of these features indicate a strong human presence associated with these horizons.

The two anthropogenic grey facies, F2b and F2c, slightly differ from one another. Facies F2c, found in three cores (Figs. 6, 7) seems to exhibit less anthropogenic impact than facies F2b, found only in core SY1. The difference is more evident when comparing F2c to sub-facies

F2b2, as F2b2 contains lower concentrations of man-made elements and micro-remains such as phytoliths and ash.

By contrast, the bounding sand facies (F2a and F2d) are clearly of aeolian origin and lack signatures of human activity. The two facies have the lowest concentrations of elements other than Si and Ca and the lowest MS values recorded in this study (below 50 $\times 10^{-8}$ m^3 Kg^{-1}). The characteristics of F2a and F2d do not suggest evidence of fire (Gvirtzman and Wieder, 2001; Tsatskin et al., 2008) or human, animal or cultivation activity.

5.2.1 The dumping site

The thickness of facies F2b (approximately 4 m), along with the internal separation by thin units of natural aeolian sand (F2a), indicates repeated activity in the same locality. Two options can explain such an assemblage of macroscopic and microscopic artefacts outside of a settlement: (a) repeated human habitation with intermittent abandonment phases, and (b) repeated garbage disposal activity with intermittent abandonment phases. The absence of architecture, combined with the placement of Facies F2b outside the walls of Roman-Byzantine Caesarea (Fig. 1d), argues against the first option. The topography of facies F2b (Fig. 6b, d), roughly 4 m higher than its surroundings, implies that this facies is in the form of a 0.07 km^2 mound (Fig. 3b, c). Thus, the topography of facies F2b indicates this accumulation may be a garbage dump.

Previous excavations have identified ancient dumps in several old cities throughout Israel. One such garbage accumulation is located in the Early Roman city of Jerusalem (Bar-Oz et al., 2013). The ancient dump in Jerusalem is rich in pottery, bone, shells, plant remains, grey building debris, coins and glass. Large garbage dumps are also known in the vicinity of Byzantine-Early Islamic (6^{th} to 9^{th} centuries CE) cities in the Negev region of southern Israel.

Preliminary observations in excavations at the ancient Negev cities of Elusa, Shivta and Nessana highlight the grey-coloured appearance of these dumps (Shahack-Gross, pers. observations). An older garbage heap in the Iron Age city of Megiddo in northern Israel is also composed of grey-coloured sediments where carbonated hydroxylapatite, phytoliths, dung spherulites and ash (along with macroscopic artefacts of pottery, bones and stones) are abundant. This Iron Age trash heap consists of several superimposed beds, indicating repeated garbage disposal activity (Shahack-Gross et al., 2009). The appearance and properties of facies F2b sediments resemble those of garbage mounds found in other cities in the southern Levant region of the Eastern Mediterranean, further evidence that facies F2b represents a garbage mound associated with ancient Caesarea (Fig. 3c).

A bone fragment obtained from the middle of facies F2b provides a temporal constraint of 662 to 774 CE. Therefore, dumping started before this date, possibly even during the Roman period. High Pb concentrations are present below the level of the dated bone fragment (Figs. 5, and 6), and high lead concentrations are generally associated with Roman period activities (Rosen and Galili, 2007). The dated bone fragment is overlain by approximately 2 m of facies F2b sediments, indicating that the garbage mound also operated after 720 CE. At 740 CE, the Muslims took control over Caesarea following a seven year siege, a conquest that did not lead to large scale destruction and abandonment (Avni, 2014). The continued use of the dumping site after the Islamic conquest appears to be represented at the top of facies F2b.

Consideration of the spatial and temporal characteristics of the landfill can assist with identifying probable users of the dumping site. This apparent urban dumping site operated 0.5 km south of the ancient wall of Byzantine Caesarea (Fig. 1d) and a few hundred meters east of the southern Bay of Caesarea. The Bay of Caesarea was a hub of maritime activity (Fig. 7d)

that included an anchorage and a pier set in the natural bay (Galili et al., 1993) in addition to a Byzantine docking site and ship cargo remains (sites 33 and 32; Fig. 7d). Therefore, users of the dumping site likely included city inhabitants and anchorage workers.

5.2.2 Modified agricultural sand south of Caesarea

Facies F2c presents a different formation process then F2b. The facies extends over a larger area in comparison to facies F2b and is thinner (reaching a maximum thickness of about 3 m; Fig. 3c). Facies F2c is somewhat less anthropogenically impacted in terms of elemental concentrations and macroscopic and microscopic artefacts (Fig. 5d). F2c is located 0.2 km from the coastline and extends up to 1.5 km landward (Fig. 7d), covering an area of 1.4 km^2 with an overall volume of about 4.8 km^3. F2c does not exhibit evidence of widespread architecture. Comparison of the underlying and overlaying natural aeolian sand units demonstrates that facies F2c has the following characteristics: (i) higher organic content; (ii) higher P, S and Ca concentrations, (iii) the presence of phytoliths, and (iv) calcitic-clay coatings surrounding the quartz sand grains.

Based on these observations, we postulate that facies F2c represents a pedo-sediment that is the outcome of aeolian sand fertilised to be suited for agricultural use. We propose that the higher organic content and elevated elemental concentrations are the result of composting practices. The compost itself may have been domestic or urban trash, which explains the presence of pottery, glass and rock fragments. The calcitic-clay coatings may indicate incipient pedogenesis (compared with the clay coatings around the quartz sand in the palaeosol; Fig. 5a, e). Such composting practices could change the barren coastal aeolian sand into a fertile sediment suited for agricultural use (Tsoar and Zohar, 1985; Ward and Summers, 1993; Blume and Leinweber, 2004). Moreover, composting added silt (Fig. 4; Table 3) to the original sand

which enhanced the water adhesion properties of the sediment. Historical reuse of organic-rich material for agricultural composting has been documented in other regions throughout the Mediterranean and the Middle East, including Crete, Greece, Egypt and Iraq, dating as far back as the third millennium (Wilkinson, 1989; Bull et al., 2001). The low number of phytoliths found in the pedo-sediment means they cannot be used for further interpretation or statistical analysis. The existence of phytoliths, however, may be a by-product of the original compost, as they are abundant in the garbage deposits identified in facies F2b.

Overall, facies F2c is interpreted as the remains of agricultural fields that supported ancient Caesarea several of centuries before 1165 ± 110 CE (Fig. 7a, c; Table 3). This interpretation is supported by historical and archaeological records. During the Roman and perhaps most of the Byzantine period, there was little attempt to conduct agricultural intensification of the immediate countryside of Caesarea (Safrai, 2003). Agricultural produce may have poured to the city not only from its port, but from villages as far as the Carmel coast to the north and east of Poleg Stream to the south (Fig. 1b; Holum, 2016). Only in the late Byzantine or the Early Islamic period was there an active attempt to improve the fertility of the sand around Caesarea for more intensive agriculture. These actions were perhaps aimed at making the huge metropolis less dependent on imports and long supply lines resulting from the politically volatile conditions of the 6th and 7th centuries CE (e.g., the 6th century revolts of the Samaritans). Three types of archaeological evidence found in the vicinity of Caesarea have led researchers to suggest that the area is surrounded by agricultural plots: (a) grey sediments in rectangular shapes, (b) excavations of farm houses and farming complexes, (c) botanical analyses of finds from Caesarea.

Porath (1975) was the first to propose that the area south of Caesarea was the focus of an intensive agricultural effort conducted by the central authorities of the city. He identified raised plots with a 0.5 to 0.7 m thick layer of grey sediment consisting of sherds, building refuse and shreds. He interpreted these plots as Mawasi agriculture (Fig. 7), as the grey sediment was situated just above the high coastal fresh water table, probably allowing natural subsurface watering by capillary rise (Warren, 1871; Tsoar and Zohar, 1985; Sánchez and Cuellar, 2016). Excavations near Or-Akiva (Fig. 1b) led Ad (2009) to suggest that the coastal agricultural system extended up to 3 km east of Caesarea. Ad proposed this hypothesis due to the presence of a similar grey-coloured sand deposit containing sherds, coins, construction materials and possibly trash remains. The trash remains may have been brought from Caesarea in order to improve the cultivation properties of the sediment. In addition, the Or-Akiva excavations contained farming complexes with a well, water dividing channels, delineation walls and a threshing floor. The archaeological evidence for agricultural intensification near Caesarea is also supported by rich archaeobotanic finds from Caesarea itself. The majority of weed and wild species found within the assemblage of edible plants are common components of field cultivation (Ramsay and Holum, 2015).

The archaeological finds and historical documentation combined with radiometric ages obtained in this study show that Caesarea had a large agricultural system that dates to the Islamic period. Dating of the pottery remains and Fatimid quarter coins excavated in the field area and archaeobotanic finds from Caesarea suggest that the fields operated throughout early Islamic times. These dated artefacts and archaeobotanic samples are supported by historical descriptions from Early Islamic period writers that praise the agricultural produce of the city (Avni, 2014; Ramsay and Holum, 2015). Other sources point out that even after the Crusader conquest, and

during the 12th century until the battle of Hattin (1101 to 1087 CE), Caesarea was still involved in agricultural production of wheat, olives, citrus and figs (Prawer, 1972; Ramsay and Holum, 2015). Recent work has identified similar grey sand units between eroded berms in the Yavne dune field (Fig. 1) along the southern coast of Israel (Roskin and Taxel, 2017). The grey units in this location have early 12th century OSL ages similar to those found in the Caesarea fields. Yavne's grey sand also displays slightly improved fertility (phosphate, potassium, nitrogen and calcium carbonate concentrations) relative to the underlying sand, suggesting an anthropogenic enrichment of ash and refuse. The Yavne finds suggests a similar and contemporaneous attempt to improve agricultural productivity during the Early Islamic period in the Israeli sandy coastal plain.

6. Conclusion

This paper provides a detailed holistic study of sediments from the southern hinterland of Caesarea, Israel in order to explore the impact of an urban settlement on its periphery. Combining sedimentological and micro-archeological analyses of recently acquired borehole data with existing topographic, chronology, log-lithology, archaeological finds and historical documentations enables the following conclusions to be made:

1. We identified two different facies of anthropogenically influenced sediments.

a. An urban garbage mound, characterised by a dark grey sediment containing the highest copper, lead and phosphate ratios found in this study, along with the presence of ash, micro-charcoal and macroscopic artefacts such as pottery and glass.

b. A cultivated 1 to 3 m thick grey pedo-sediment covering an area of 1.4 km^2, identified by the presence of higher organic content, phosphate, sulphur and calcite ratios compared to underlying and overlying natural sand, along with plant phytoliths.

The ability to differentiate between anthroposols through the holistic approach presented in this study could be used in future research to reveal past uses of landscapes and soils.

2. During the early Islamic period, inhabitants of Caesarea enriched the nutrient deprived sediments south of the city by adding domestic or urban refuse. These composting practices changed the barren coastal aeolian sand into a fertile pedo-sediment with water adhesion properties better suited for agricultural use.
3. The burial of the agricultural pedo-sediment, signifies the end of the cultivation period, dates to the Crusade period. This chronology agrees with historical evidence of the decline and abandonment of Caesarea.

This study shows the potential for studying hinterlands of urban centres through analysis of sediment cores in addition to conventional archaeological work that typically focuses on excavation of settlements. It is likely that sites with similar anthropogenic pedo-sediments are present along the coast of Israel. However, because such sites have not yet been explored through the methodologies used in this research, it is unclear whether fertilizing sandy sediments was pioneered in Caesarea or if it was part of a wider (possibly earlier) phenomenon. The holistic approach presented here may offer new possibilities to increased understanding of the impact of human societies on the environment.

Acknowledgments

The authors gratefully acknowledge support from the University of Haifa, the Helmsley Charitable Trust Mediterranean Sea Research Center, and also Maurice and Lady Hatter Fund of the Leon Recanati Institute for Maritime Studies (RIMS) at the University of Haifa. Dina Dagan Begun of Ben Gurion University of the Negev and Silas Dean, Benny Bechor and Dr. Guy Sisma-Ventura of the University of Haifa are thanked for their vital help in the field. We also thank Dr. Or M. Bialik and Dr. Nimer Taha from the University of Haifa for their help in the sedimentological and geochemical analyses. Jonathan J. Gottlieb from the University of Haifa is thanked for preparation of thin sections. Improvements of earlier versions of the manuscript by two anonymous reviewers and by Associate Editor Dr Veerle Vanacker are truly appreciated.

.

References

1. Ackermann, O., Greenbaum, N., Ayalon, A., Bar-Matthews, M., Boaretto, E., Bruins, H.J., Cabanes, D., Horwitz, L.K., Neumann, F.H., Porat, N., Weiss, E., Maeir, A.M., 2015. Using palaeo-environmental proxies to reconstruct natural and anthropogenic controls on sedimentation rates, Tell es-Safi/Gath, eastern Mediterranean. Anthropocene 8, 70-82.
2. Ackermann, O., Greenbaum, N., Bruins, H., Porat, N., Bar-Matthews, M., Almogi-Labin, A., Schilman, B., Ayalon, A., Horwitz, L.K., Weiss, E., Maeir, A.M., 2014. Palaeoenvironment and anthropogenic activity in the southeastern Mediterranean since the mid-Holocene: The case of Tell es-Safi/Gath, Israel. Quaternary International 328-329, 226-243.
3. Ad, U., 2009. Or-Akiva: Remains of a Farming Complex and Irrigation System from the End of the Byzantine–Beginning of the Early Islamic Periods in the Agricultural Hinterland of Caesarea. Atiqot 61, 49-60 (in Hebrew).
4. Adams, A.E., MacKenzie, W.S., 1998. A color atlas of carbonate sediments and rocks under the microscope. Manson Publishing Ltd., London, UK.

5. Almagor, G., Gill, D., Perath, I., 2000. Marine Sand Resources Offshore Israel. Marine Georesources & Geotechnology 18, 1-42.

6. Avni, G., 2014. The Byzantine-Islamic transition in Palestine: an archaeological approach. Oxford University Press.

7. Bar-Oz, G., Bouchnik, R., Weiss, E., Weissbrod, L., Bar-Yosef Mayer, D.E., Reich, R., 2013. "Holy Garbage": A Quantitative Study of the City-Dump of Early Roman Jerusalem. Levant 39, 1-12.

8. Bar-Matthews, M., Ayalon, A., Gilmour, M., Matthews, A., Hawkesworth, C.J., 2003. Sea–land oxygen isotopic relationships from planktonic foraminifera and speleothems in the Eastern Mediterranean region and their implication for paleorainfall during interglacial intervals. Geochimica et Cosmochimica Acta 67, 3181-3199.

9. Bar-Yosef, O., 1975. The Epi-paleolithic in Palestine and Sinai, In: Marks, A.E. (Ed.), Problems in prehistory: North Africa and the Levant. SMU Press, Dallas, Texas pp. 363-378.

10. Blume, H.-P., Leinweber, P., 2004. Plaggen Soils: landscape history, properties, and classification. Journal of Plant Nutrition and Soil Science 167, 319-327.

11. Bouma, J., Hole, F.D., 1971. Soil structure and hydraulic conductivity of adjacent virgin and cultivated pedons at two sites: A Typic Argiudoll (silt loam) and a Typic Eutrochrept (clay). Soil Science Society of America Journal 35, 316-319.

12. Box, M.R., Krom, M.D., Cliff, R.A., Bar-Matthews, M., Almogi-Labin, A., Ayalon, A., Paterne, M., 2011. Response of the Nile and its catchment to millennial-scale climatic change since the LGM from Sr isotopes and major elements of East Mediterranean sediments. Quaternary Science Reviews 30, 431-442.

13. Bull, I., Phillip PB, Richard PE, 2001. An Organic Geochemical Investigation of te Practice of Manuring at a Minoan Site on Pseira Island, Crete. Geoarchaeology 16, 223-242.

14. Certini, G., Scalenghe, R., 2011. Anthropogenic soils are the golden spikes for the Anthropocene. The Holocene 21, 1269-1274.

15. Cohen-Seffer, R., Greenbaum, N., Sivan, D., Jull, T., Barmeir, E., Croitoru, S., Inbar, M., 2005. Late Pleistocene–Holocene marsh episodes along the Carmel coast, Israel. Quaternary International 140-141, 103-120.

16. Danin, A., 2005. The sandy areas of Caesarea, a rare situation of alpha and beta diversity linked by plant succession. Israel Journal of Plant Sciences 53, 247-252.
17. Davis, M., Matmon, A., Rood, D.H., Avnaim-Katav, S., 2012. Constant cosmogenic nuclide concentrations in sand supplied from the Nile River over the past 2.5 my. Geology 40, 359-362.
18. Ellenblum, R., 2012. The collapse of the eastern Mediterranean: climate change and the decline of the East, 950-1072. Cambridge University Press.
19. Emery, K., Neev, D., 1960. Mediterranean beaches of Israel: Israel Geological Survey Bulletin. 26, 1-24.
20. Engelmann, A., Neber, A., Frechen, M., Boenigk, W., Ronen, A., 2001. Luminescence chronology of Upper Pleistocene and Holocene aeolianites from Netanya South - Sharon Coastal Plain, Israel. Quaternary Science Reviews 20, 799-804.
21. Frechen, M., Dermann, B., Beonigk, W., Ronen, A., 2001. luminesence chronology of the aeolianites from the section at givat olga-coastal plain of israel. Quaternary Science Reviews 20, 805-809.
22. Frechen, M., Neber, A., Dermann, B., Alexander, T., Boenigk, W., Raban, A., 2002. Chronostratigraphy of aeolianites fromthe Sharon Coastal Plain of Israel. Quaternary International, 31-44.
23. Frechen, M., Neber, A., Tsatskin, A., Boenigk, W., Ronen, A., 2004. Chronology of Pleistocene sedimentary cycles in the Carmel Coastal Plain of Israel. Quaternary International 121, 41-52.
24. Galili, E., Dahari, U., Sharvit, J., 1993. Underwater surveys and rescue excavations along the Israeli coast. The International Journal of Nautical Archaeology 22, 61-77.
25. Galili, E., Nir, Y., 1993. The submerged Pre-Pottery Neolithic water well ofAtlit-Yam, northern Israel and its palaeoenviromental implications. The Holocene 3, 265-270.
26. Godfrey-Smith, D.I., Vaughan, K.B., Gopher, A., Barkai, R., 2003. Direct luminescence chronology of the Epipaleolithic Kebaran site of Nahal Hadera V, Israel. Geoarchaeology 18, 461-475.
27. Goodman-Tchernov, B.N., Austin, J.A., 2015. Deterioration of Israel's Caesarea Maritima's ancient harbor linked to repeated tsunami events identified in geophysical mapping of offshore stratigraphy. Journal of Archaeological Science: Reports 3, 444-454.

28. Gvirtzman, G., Netser, M., Katsav, E., 1998. Last-Glacial to Holocene kurkar ridges, hamra soils, and dune fields in the coastal belt of central Israel. Israel Journal of Earth Sciences 47, 27-46.

29. Gvirtzman, G., Wieder, M., 2001. Climate of the last 53,000 years in the eastern med based on soil-sequence Stratigraphy in coastla plain Israel. Quaternary Science Reviews 20, 1827-1849.

30. Habas, E., 1996. The Halachic status of Caesarea as reflected in the Talmudic literature, In: Raban A, KG, H. (Eds.), Caesarea Maritima: a retrospective after two millennia, Brill, Leiden, pp. 454-475.

31. Hole, F., 1974. Wild soils of the Pine-Popple Rivers basin. Transactions of the Wisconsin Academy of Sciences, Arts, and Letters.

32. Holum, K.G., 2009. Et dispositione civitatis in multa eminens: Comprehending the urban plan of 4th century Caesarea. Man near a Roman arch. The Israel Exploration Society, Jerusalem, 187-207.

33. Holum, K.G., 2011. Caesarea Palaestinae: a paradigmatic transition. Shaping the Middle East. Jews, Christians, and Muslims in an Age of Transition, 400-800.

34. Holum, K.G., 2016. Caesarea Palaestinae: City and Countryside in Late Antiquity: City and Countryside in Late Antiquity, In: Patrich, J., Peleg-Barkat, O., Ben-Yosef, E. (Eds.), Arise, Walk Through the Land. Studies in the Archaeology and History of the Land of Israel in Memory of Yizhar Hirschfeld on the Tenth Anniversary of his Demise. Israel Exploration Society, Jerusalem, pp. 1-16.

35. Israel Meteorological Service, 2011. Climate Atlas, http://www.ims.gov.il/IMS/CLIMATE/ClimaticAtlas/RainMaps.htm (16.02.15) (in Hebrew).

36. Kadosh, D., Sivan, D., Kutiel, H., Weinstein-Evron, M., 2004. A late quaternary paleoenvironmental sequence from Dor, Carmel coastal plain, Israel. Palynology 28, 143-157.

37. Kutiel, P. B., Katz, O., Ziso-Cohen, V., Divinsky, I., Katra, I., 2016. Water availability in sand dunes and its implications for the distribution of Artemisia monosperma. Catena, 137, 144-151.

38. Langgut, D., Almogi-Labin, A., Bar-Matthews, M., Weinstein-Evron, M., 2011. Vegetation and climate changes in the South Eastern Mediterranean during the Last Glacial-Interglacial cycle (86 ka): new marine pollen record. Quaternary Science Reviews 30, 3960-3972.

39. Levin, N., 2013. The Palestine exploration fund map (1871–1877) of the holy land as a tool for analysing landscape changes: the coastal dunes of Israel as a case study. The Cartographic Journal.

40. Mauz, B., Hijma, M.P., Amorosi, A., Porat, N., Galili, E., Bloemendal, J., 2013. Aeolian beach ridges and their significance for climate and sea level: Concept and insight from the Levant coast (East Mediterranean). Earth-Science Reviews 121, 31-54.

41. Neev, D., Schanai, E., Hall, J.K., Bakler, N., Ben-Avraham, Z., 1978. The Young (Post Loewr Pliocene) Geological History of the Caesarea. Israel Journal of Earth Sciences 28, 43-46.

42. Nicosia, C., Devos, Y., 2014. Urban dark earth, Encyclopedia of Global Archaeology. Springer, pp. 7532-7540.

43. Olami, Y., Sender, S., Oren, E., 2005. Map of Binyamina. Israel Antiquities Authority, Jerusalem.

44. Patrich, J., 2001. The carceres of the Herodian hippodrome/stadium at Caesarea Maritima and connections with the Circus Maximus. Journal of Roman Archaeology 14, 269-283.

45. Picard, L., 1943. Structure and evolution of Palestine. Bull. Geol. Dept. Hebrew Univ., Jerusalem 4, 1-134.

46. Pomerancblum, M., 1966. The distribution of heavy minerals and their hydraulic equivalents in sediments of the Mediterranean continental shelf of Israel. Journal of Sedimentary Research 36.

47. Porat, N., Wintle, A.G., Ritte, M., 2004. Mode and timing of kurkar and hamra formation, central coastal plain, Israel. Israel Journal of Earth Sciences 53, 13-25.

48. Porath, Y., 1975. The Gardens of Caesarea. Qadmoniot, 30-31.

49. Porath, Y., 2000. Caesarea–1994–1999. Hadashot Arkheologiyot: Excavations and Surveys in Israel (in Hebrew), 34-40.

50. Porath, Y., 2002. The water-supply to Caesarea: a re-assessment, In: Amit D, Hirschfeld Y, J, P. (Eds.), JOURNAL OF ROMAN ARCHAEOLOGY-SUPPLEMENTARY SERIES, pp. 104-129.

51. Prawer, J., 1972. The Latin Kingdom of Jerusalem: European Colonialism in the middle Ages Weidenfeld, London.

52. Raban, A., 2007. Ancient harbors of the Mediterranean, In: Artzy M, Goodman B, Gal Z (Eds.), The Harbor of Sebastos in its Roman Mediterranean context. BAR International Series, Oxford, pp. 1-48.

53. Ramsay, J., Holum, K., 2015. An archaeobotanical analysis of the Islamic period occupation at Caesarea Maritima, Israel. Vegetation History and Archaeobotany 24, 655-671.

54. Ramsey, C.B., Lee, S., 2013. Recent and planned developments of the program OxCal. Radiocarbon 55, 720-730.

55. Regev, L., Cabanes, D., Homsher, R., Kleiman, A., Weiner, S., Finkelstein, I., Shahack-Gross, R., 2015. Geoarchaeological Investigation in a Domestic Iron Age Quarter, Tel Megiddo, Israel. Bulletin of the American Schools for Oriental Research (BASOR) 374, 135-157.

56. Reimer, P.J., Baillie, M.G., Bard, E., Bayliss, A., Beck, J.W., Blackwell, P.G., Bronk, R.C., Buck, C.E., Burr, G.S., Edwards, R.L., 2009. IntCal09 and Marine09 radiocarbon age calibration curves, 0-50,000 years cal BP. Radiocarbon 51, 1111-1150.

57. Reinhardt, E.G., Raban, A., 1999. Destruction of Herod the Great's harbor at Caesarea Maritima, Israel-Geoarchaeological evidance. Geology 27, 811-814.

58. Reinhardt, E.G., Raban, A., 2008. Site formation and stratigraphic development of Caesarea's ancient harbor, In: Holum, K., Stabler, J., Reinhardt, E. (Eds.), Caesarea Reports and Studies: Excavations 1995–200, pp. 155-182.

59. Revel, M., Ducassou, E., Grousset, F.E., Bernasconi, S.M., Migeon, S., Revillon, S., Mascle, J., Murat, A., Zaragosi, S., Bosch, D., 2010. 100,000 Years of African monsoon variability recorded in sediments of the Nile margin. Quaternary Science Reviews 29, 1342-1362.

60. Rosen, B., Galili, E., 2007. Lead Use on Roman Ships and its Environmental Effects. International Journal of Nautical Archaeology 36, 300-307.

61. Roskin, J., Sivan, D., Bookman, R., Porat, N., Shtienberg, G., 2016. Beach buildup and coastal aeolian sand incursions off the Nile cell during the Holocene Poster presented in the annual IGRG Congress; the University of Haifa, 33.

62. Roskin, J., Sivan, D., Shtienberg, G., Roskin, E., Porat, N., Bookman, R., 2015. Natural and human controls of the Holocene evolution of the beach, aeolian sand and dunes of Caesarea (Israel). Aeolian Research 19, 65-85.

63. Roskin, J., Sivan, D., Shtienberg, G., Porat, N., Bookman, R., 2017. Holocene beach build up and coastal aeolian sand incursions off the Nile littoral cell. In EGU General Assembly Conference Abstracts 19, 2391.

64. Roskin, J., Taxel, I., 2017. Early Islamic inter-settlement agroecosystems in coastal sand, Yavneh dunefield, eastern Mediterranean coast, Israel, In: EGU General Assembly Conference Abstracts 19, 844.

65. Safrai, Z., 2003. The Economy of Roman Palestine. Routledge.

66. Salmon, Y., 2013. A Second Millennium Geo-archaeological and Palaeo-environmental Study of the Nami Region: An Integrated Approach to a Coastal and Maritime Study, The Department of Maritime Civilizations. The University of Haifa.

67. Sánchez, R., Cuellar, M., 2016. Coastal interdune agroecosystems in the Mediterranean: a case study of the Andalusian navazo. Agroecology and Sustainable Food Systems 40, 895-921.

68. Sandor, A., Gersper, P.L., Hawley, J.W., 1990. Prehistoric agricultural terraces and soils in the Mimbres area, New Mexico. World Archaeology 22, 70-86.

69. Schattner, U., Lazar, M., Tibor, G., Ben-Avraham, Z., Makovsky, Y., 2010. Filling up the shelf — A sedimentary response to the last post-glacial sea rise. Marine Geology 278, 165-176.

70. Shahack-Gross, R., Ayalon, A., 2013. Stable carbon and oxygen isotopic compositions of wood ash: an experimental study with archaeological implications. Journal of Archaeological Science 40, 570-578.

71. Shahack-Gross, R., Berna, F., Karkanas, P., Weiner, S., 2004. Bat guano and preservation of archaeological remains in cave sites. Journal of Archaeological Science 31, 1259-1272.

72. Shahack-Grass, R., Gafri, M., Finkelstein, I., 2009. Identifying threshing floors in the archaeological record: a test case at Iron Age Tel Megiddo, Israel. Journal of Field Archaeology 34, 171-184.

73. Shtienberg, G., Dix, J.K., Roskin, J., Waldmann, N., Bookman, R., Bialik, O.M., Porat, N., Taha, N., Sivan, D. New perspectives on coastal landscape reconstruction during the Late Quaternary: A test case from central Israel. Palaeogeography, Palaeoclimatology, Palaeoecology 468, 503-519.

74. Shtienberg, G., Dix, J., Waldmann, N., Makovsky, Y., Golan, A., Sivan, D., 2016. Late-Pleistocene evolution of the continental shelf of central Israel, a case study from Hadera. Geomorphology 261, 200-211.

75. Sivan, D., Lambeck, K., Toueg, R., Raban, A., Porath, Y., Shirman, B., 2004. Ancient coastal wells of Caesarea Maritima, Israel, an indicator for relative sea level changes during the last 2000 years. Earth and Planetary Science Letters 222, 315-330.

76. Sivan, D., Porat, N., 2004. Evidence from luminescence for Late Pleistocene formation of calcareous aeolianite (kurkar) and paleosol (hamra) in the Carmel Coast, Israel. Palaeogeography, Palaeoclimatology, Palaeoecology 211, 95-106.

77. Sivan, D., Widowinski, S., Lambeck, K., Galili, E., Raban, A., 2001. Holocene sea level changes based on archeological sites off northen israel Palaeogeography, Palaeoclimatology, Palaeoecology 167, 101-117.

78. Smejda, L., Hejcman, M., Horak, J., Shai, I., 2017. Ancient settlement activities as important sources of nutrients (P, K, S, Zn and Cu) in Eastern Mediterranean ecosystems– The case of biblical Tel Burna, Israel. Catena, 156, 62-73.

79. Stieglitz, R., 1996. Stratonos Pyrgos - MigdalSar - Sebastos: history and archaeology, In: Rabban, A., Holum, K.G. (Eds.), Caesarea Maritima - retrospective after two millennia. Brill, Leiden, pp. 593-608.

80. Stuiver, M., Polach, H.A., 1977. Discussion; reporting of C-14 data. Radiocarbon 19, 355-363.

81. Taxel, I., 2013. The Byzantine-early Islamic transition on the Palestinian coastal plain: a re-evaluation of the archaeological evidence. Semitica et Classica, 73-106.81. Tsartsidou, G., Lev-Yadun, S., Efstratiou, N., Weiner, S., 2008. Ethnoarchaeological study of phytolith assemblages from an agro-pastoral village in Northern Greece (Sarakini): development and

application of a Phytolith Difference Index. Journal of Archaeological Science 35, 600-613.

82. Tsatskin, A., Gendler, T.S., Heller, F., Ronen, A., 2008. Near-surface paleosols in coastal sands at the outlet of Hadera stream (Israel) in the light of archeology and luminescence chronology. Journal of Plant Nutrition and Soil Science 171, 524-532.
83. Tsoar, H., Zohar, Y., 1985. Desert Dune Sand and its Potential for Modern Agricultural Development, in: Desert Development Springer, Netherland, pp. 184-200.
84. Ward, S.C., Summers, R.N., 1993. Modifying sandy soils with the fine residue from bauxite refining to retain phosphorus and increase plant yield. Fertilizer Research, 151-156.
85. Warren, C., 1871. The Plain of Philistia. Palestine Exploration Quarterly 3, 82-96.
86. Weiner, S., 2010. Microarchaeology: beyond the visible archaeological record. Cambridge University Press.
87. Wilkinson, T.J., 1989. Extensive Sherd Scatters and Land Use Intensity: Some Recent Results. Journal of Field Archaeology 16, 31-46.
88. Wright, V., 1992. A revised classification of limestones. Sedimentary Geology 76, 177-185.
89. Wright, C.I., Tucker, M.E., 1991. Calcretes. Blackwell Scientific Publications, Oxford, UK.
90. Yaalon, D.H., 1967. Factors affecting the lithification of eolianite and interpretation of its environmental significance in the coastal plain of Israel. Journal of Sedimentary Research 37, 1189-1199.
91. Yaalon, D.H., Dan, J., 1967. Factors controlling soil formation and distribution in the Mediterranean coastal plain of Israel during the Quaternary. Quaternary soils, 321-338.
92. Zeder, M.A., 2011. The Origins of Agriculture in the Near East. Current Anthropology 52, S221-S235.
93. Zviely, D., Kit, E., Rosen, B., Galili, E., Klein, M., 2009. Shoreline migration and beach-nearshore sand balance over the last 200 years in Haifa Bay (SE Mediterranean). Geo-Marine Letters 29, 93-110.
94. Zviely, D., Sivan, D., Ecker, A., Bakler, N., Rohrlich, V., Galili, E., Boarreto, E., Klein, M., Kit, E., 2006. Holocene evolution of the Haifa Bay area, Israel, and its influence on ancient tell settlements, The Holocene, pp. 849-861.

Figure caption:

Figure 1: Regional and sedimentological context of the study area. (a) Map of the southeast Mediterranean illustrating the Nile littoral cell and longshore transport responsible for accumulation of sand along the eastern Mediterranean Israeli coast. (b) Detailed map showing sand sheets and Late Pleistocene aeolianite ridges typical to Israel's coastal plain and the river systems flowing toward the coastal area. (c) Map of the Caesarea area (study site) marking previously published and current boreholes along with dated unit locations. (d) Map of Caesarea (32°30'0" N, 34°53'30" E) annotating the previously excavated site and harbour ruins (modified after Reinhardt and Raban, 2008) in relation to borehole SY1 on a rectified aerial photograph from 2016.

Figure 2: Site morphology of the coastal area south of Caesarea. The site location is displayed in Figure 1c. (a) Rectified aerial photograph (Orthophoto) from 2016 annotating the northern boundary of the agricultural plots. (b) Rectified aerial photograph from 1946 annotating the northern boundary of the agricultural plots. (c) DEM of the coastal area south of the northern boundary of the agricultural hinterland and southern aeolianite ridge. (d) Photograph of an agricultural plot surrounded by berms. The location is displayed in Figure 2c (red rectangle). (e) Grey sand rich with sherds, marble, seashells and glass covering the berm surface.

Figure 3: Elevation and sediment thickness maps. (a) The bottom elevation of the yellow sand facies. (b) The thickness of the entire sandy unit (c) The thickness of the grey sand facies interpolated from the presented boreholes (red dot). Note that the grey sand facies covers a large area south and southeast of Caesarea, with the thickest part located closest to the ancient city walls.

Figure 4: Detailed information obtained from boreholes SY1, SDC1, SDC2 and SDC4. Note that grey lithological units seem to correspond with increased silt levels, increased magnetic susceptibility, and presence of phosphate-containing minerals.

Figure 5: Microscopic features in thin section (a-e) and macroscopic finds (f). (a) Unit F1 (palaeosol). Subrounded quartz grains (red arrow) within a groundmass of reddish-brown clay. (b) Sub-unit F2d (yellow sand). Subrounded quartz grains (red arrow) and skeleton of the foraminifer Textulariidae sp. (yellow arrow) testifying to the aeolian origin of this unit. (c) Sub-unit F2b (grey sand) with a bone fragment and micro-charcoal fragments (red arrow). (d) Sub-unit F2b (grey sand). Low quantities of quartz grains associated with abundant micro-charcoal fragments (green arrow), phytoliths (purple arrow), pollen grains (blue arrow) and micritic calcite resembling wood ash (yellow arrow). (e) Unit F2c (grey sand). Quartz grains partly surrounded by dark microsparitic calcite. (f) Glass (1) and pottery remains (2-4) which were identified throughout sub-units F2b and F2c. Note that artefacts and microscopic remains indicating human activity are primarily identified in the grey sand sub-unit F2b.

Figure 6: Relative elemental concentrations (all normalized relative to silicon concentrations) measured in boreholes SY1, SDC1 and SDC2. The various lithofacies are presented along with macroscopic remains found within them. A bone (borehole SY1) fragment yielded a radiocarbon date that is presented here as well, corresponding to the Early Islamic period. Note that the trace element values for Cu in borehole SDC1 and Cu and Pb in borehole SDC2 (marked by asterisk) were lower than the detection capabilities of the EX-310LC(ED) instrument.

Figure 7: Chronostratigraphic cross sections in the coastal area south of Caesarea (a-c) based on previous lithological and OSL data (marked with a star) published in Roskin et al. (2015) as well as lithological and radiocarbon data from this study which are both annotated relevant to

Common Era. Refer to (d) to follow cross sections in space. The modern topography of the area was extracted from the 4 × 4 m DEM. Archaeological sites (black stars in d) are marked with a site number linked to the IAA survey: http://www.antiquities.org.il/survey/new/.

Note that OSL dates determine the date of last exposure to sunlight, while radiocarbon dates indicate the time of death of organic matter.

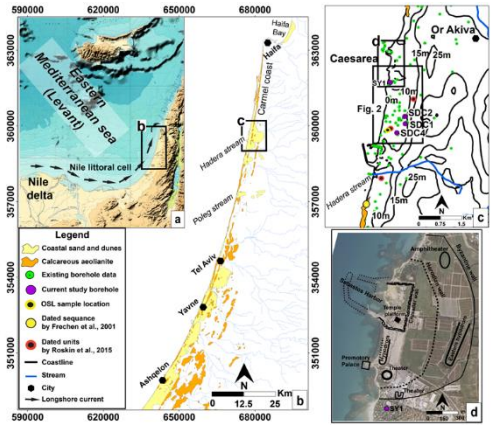

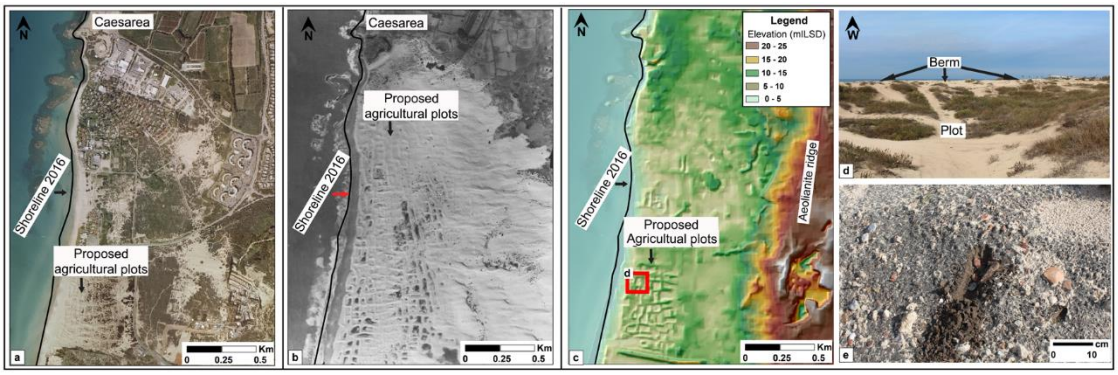

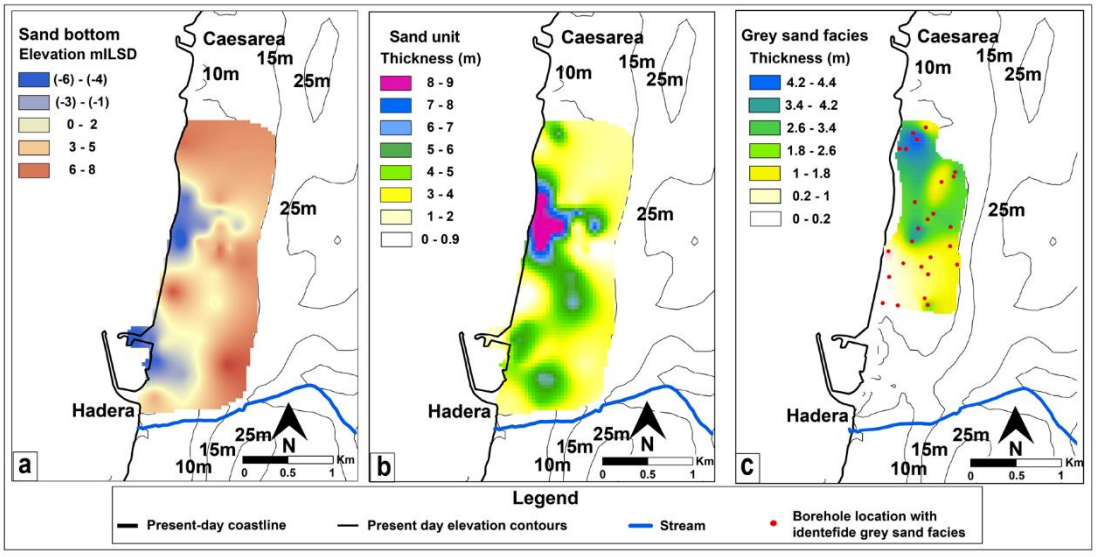

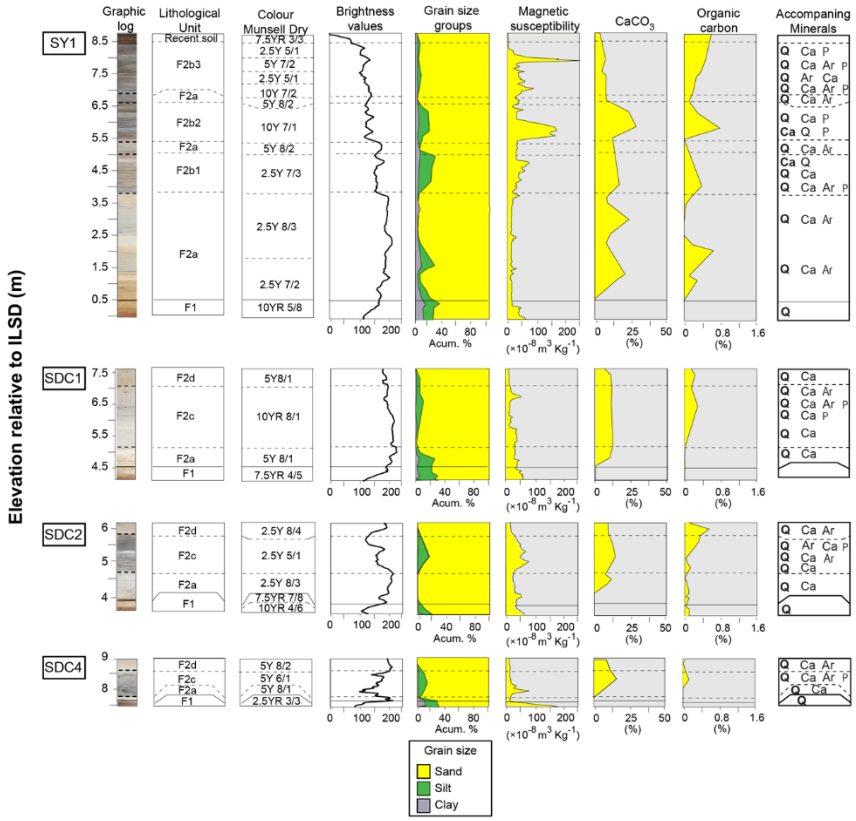

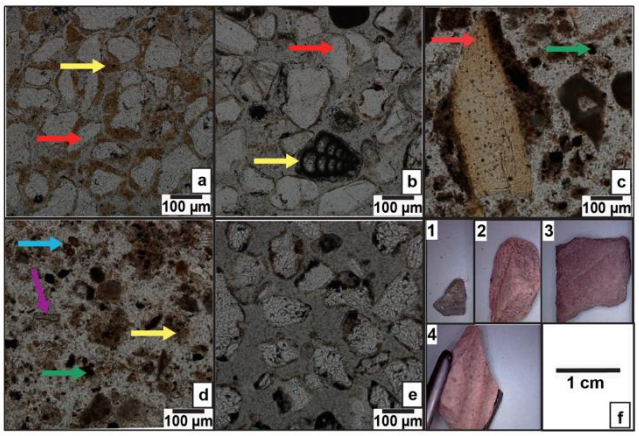

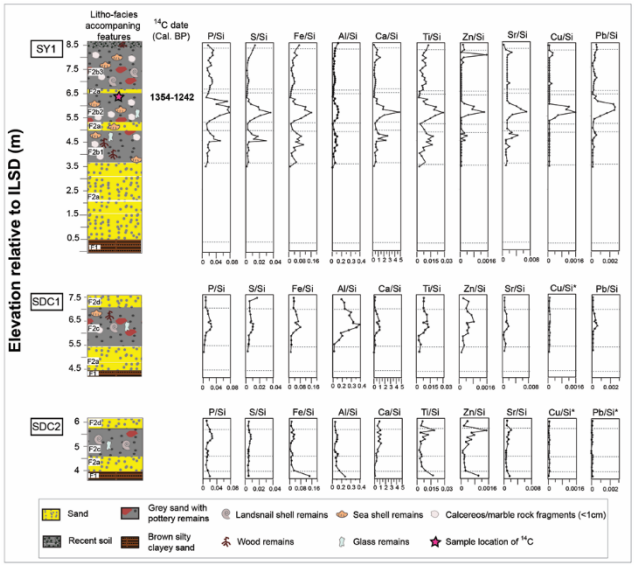

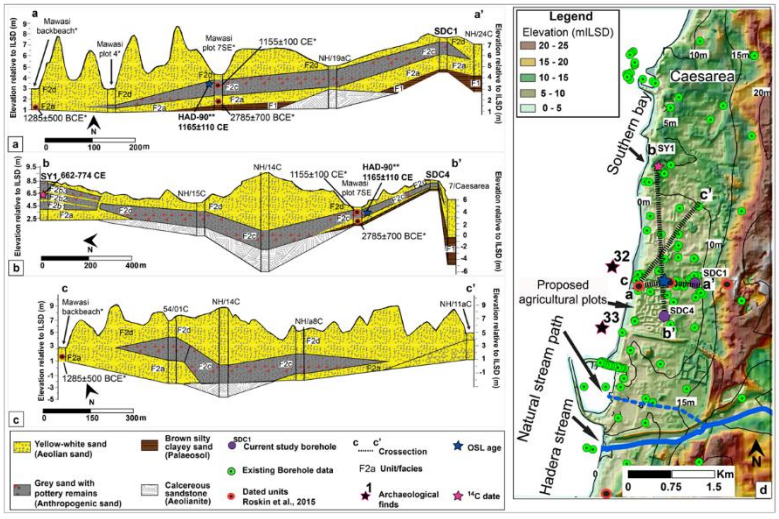

Table 1: Optically stimulated luminescence (OSL) laboratory data and age with corresponding lithological facies, sample depth relative to ILSD (m) and sample location (UTM). The sample was measured in 2-mm aliquots. The De and error on De were calculated using unweighted mean and standard deviation. The sample shows recycling ratios within 5% of 1.0 and negligible recuperation and IR signals. Aliquots used: the number of aliquots used for the average De out of the aliquots measured.

Sample name	Est. moisture (%)	Facies grain size (µm)		Elev. (mILSD)	location (UTM 36N)	K (%)	U (ppm)	Th (ppm)	Ext. α (µGy/a)	Ext. β (µGy/a)	Ext. γ (µGy/a)	Cosmic (µGy/a)	Total dose (µGy/a)	No. of discs	OD (%)	De (Gy)	**Age (ka)**
HAD-90	3	Grey clayey sand 90-125		4	677775 3595235	0.39	0.57	1.24	2	367	211	176	757±20	18/19	21	0.64±0.09	**0.85±0.11**

Table 2: Radiocarbon ages of the two samples from the cores SY1 and SDC1 at different depths: the bone remains and wood fragments both retrieved from a grey sand at depths of 6.5 and 5.5 m respectively. The ages are given as ^{14}C age ± 1s year BP, and the calibrated ranges for ±1s and ±2s in years BP, according to the convention in Stuiver and Polach (1977).

Core	Lab no.	Elev. (mILSD)	Location (UTM 36N)	Material	^{14}C age ±1σ year BP uncal.	Calibrated range ± 1σ year BP	Calibrated range ±2σ year BP
SY1	Poz-83568	6.5	677740 3596659	Bone remains in grey sand unit	1280 ± 30 BP	1335 (40.8%) 1295 1275 (27.4%) 1249	1354 (95.4%) 1242
SY1	Poz-83569	4.7	677740 3596659	Wood fragments in grey sand unit	Modern	64 (68.2%) 60	66 (95.4%) 58
SY1	Poz-83571	4.5	677740 3596659	Wood fragments in grey sand unit	Modern	64 (68.2%) 60	66 (95.4%) 58
SDC1	Poz-83570	6.8	678109 3595207	Wood fragments in grey sand unit	Modern	64 (68.2%) 60	66 (95.4%) 57

Table 3: Characterisation and chronology of the sedimentological unit identified in the current study from the surface downward

Unit	Facies	Sub-facies	Grain texture	Accompanying features	Unit interpretation	OSL (ka)	Cal. ^{14}C age (BP)	Historical date (BCE/CE)	Cultural period	Reference (ages)
F2	F2d	-	Sand	Subrounded quartz grains, land snail fragments	Sand	present to 0.65 ± 0.16		present to 1365 ± 160 CE	Israel - Mameluke - Ottoman Empire	Frechen et al., 2001; Salmon, 2013; Roskin et al., 2015
	F2c	-	Loamy sand	Subrounded quartz grains surrounded with dark microsparitic calcite, pottery remains, 0.5 cm calcareous sandstone rocks, shell and land snail fragments, glass remains	Anthropogenic sand	0.85 ± 0.11; 0.86 ± 0.1		1165 ± 110 CE; 1155 ± 100 CE	Crusader	Current study; Roskin et al., 2015
	F2b	3	Sand	1 cm calcareous sandstone rocks, land snail and shell fragments, wood ash, micro charcoal	Anthropogenic sand					
		2	Loamy sand	Phytoliths, sherds, 1 cm calcareous sandstone rocks, wood pieces, shells, bone pieces, wood ash, micro charcoal, glass fragments	Anthropogenic sand		1354 – 1242	774 – 662 CE	Early Islamic	Current study
		1	Loamy sand	Phytoliths, sherds, 1 cm calcareous sandstone rocks, wood pieces, shells glass fragments	Anthropogenic sand					
	F2a	-	Sand	Subrounded quartz grains shell and land snail fragments, microfossil remains	Sand	3.3 ± 0.5 to 5.9 ± 0.9		1285 ± 500 to 3885 ± 900 BCE	Chalcolithic - Bronze age	Frechen et al., 2002; Kadosh et al., 2004; Porat et al., 2004; Cohen-Seffer et al., 2005; Mauz et al., 2013; Roskin et al., 2015; Shtienberg et al., 2017
F1	-	-	Sandy loam	Subrounded to rounded quartz grains and groundmass of reddish-brown clay	Palaeosol (unit upper constrain)	7.7 ± 1.2		~6000 BCE	Neolithic	Gvirtzman and Wieder, 2001; Roskin et al., 2016